Hole bipolaron formation at (100) MgO/CaO epitaxial interface

N. Bondarenko,[1] O. Eriksson,[1] and N. V. Skorodumova[1,2]

[1]*Department of Physics and Astronomy, Uppsala University, Box 516, 75121 Uppsala, Sweden*

[2]*Multiscale Materials Modelling, Department of Materials Science and Engineering, Royal Institute of Technology, SE-100 44 Stockholm, Sweden*

(Received 2 December 2013; revised manuscript received 20 February 2014; published 19 March 2014)

Hole localization accompanying the formation of a cation vacancy in bulk MgO and CaO and at the (100) MgO/CaO interface is described using the Heyd-Scuseria-Ernzerhof hybrid functionals and DFT + U method. The ground state is found to be the O^1-O^1 bipolaronic configuration both in bulk oxides and at their interfaces. The ground-state magnetic configuration is a triplet, which has an energy only about 1–2 meV lower than that of the singlet state. The one-centered O^2-O^0 bipolaron was found to be metastable with its stability being enhanced at the interfaces compared to that in bulk oxides. Possible transition between different biplaronic configurations at the interface are analyzed for chosen configurations.

DOI: 10.1103/PhysRevB.89.125118 PACS number(s): 31.15.A−

I. INTRODUCTION

Charge redistribution and localization in defective oxides is a phenomenon both important for applications and challenging for theoretical description. Charge localization can occur in a solid when the charge-lattice interaction is large so charge can get "trapped" by local lattice deformation. Such complex objects of a localized charge, with lattice distortions associated with it are often called polarons, a concept first introduced by Landau in 1933 [1]. These quasiparticles became a subject of intensive theoretical studies [2–6] due to their importance for numerous phenomena observed in different materials [7–9]. Polarons appear in a large number of oxides, molecular solids, and organic compounds. The interest to polarons and their mobility in oxides in particular is fuelled by their high relevance to different applications ranging from lithium batteries [10], fuel [11,12] and solar cells [13] to superconductors [9].

Both "continuum" and "discret" models of polarons developed up to date [3,4] provide us with the knowledge of general characteristics of polaronic systems depending on the kind of the carrier-lattice interactions, long- or short-range, dimensionality of the system and other criteria [14–18]. Within such approximations, the polarons can be formally divided into two main subcategories: "large" polarons that are spread over the supporting media in contrast to strongly onsite localized, "small" polarons. Both "continuum" and "discret" models describing "*small*" and "large" polarons can be found in numerous publications and reviews on the subject, see, for example, Refs. [5,6].

Recently, a number of reports of the first-principles calculations of polarons in different materials have appeared. For example, both electron and hole polarons have been described in ionic oxides, such as pure and doped MgO [19], ZnO [20,21], SiO_2 [22], CeO_2 [11,12,23], TiO_2 [24–28], HfO_2 [29,30], $LiFePO_4$ [10], $LiNbO_3$ [31], $Nd_{2-x}Ce_xCuO_4$ [14], Li_2O_2, and Li_2CO_3 [32,33]. The common conclusion of these studies is that in order to correctly reproduce the charge localization and associated lattice distortion one needs to use methods going beyond conventional local and semilocal approximations of density functional theory (DFT), such as DFT + U [10,24,27,34], Self interaction correction (SIC) [34], hybrid functionals [25,33,34] or dynamic mean-field theory (DMFT) [18]. In alkaline earth oxides, hole polarons can form when cation vacancies, also called V centers, or aliovalent impurities are present [35]. It appears to be established by both experiment [36–41] and theory [41,42] that the formation of a cation vacancy in these oxides is accompanied by hole localization in an O^1-O^1 bipolaronic configuration, namely, at two oxygen atoms on opposite sides of the cation vacancy, as illustrated in Fig. 1.

The localized holes possess local magnetic moments, which could be either parallel (triplet state) or antiparallel (singlet state) to each other. The magnetic state of trapped holes in MgO and CaO was debated in the literature [34,36–39,41,43] Some experiments showed the triplet ($S = 1$) to be the ground state for MgO [38,44], whereas others did not confirm it [36]. For CaO, experiments indicated the dominance of the singlet state ($S = 0$) [39,45]. These investigations showed that neutral vacancies (V^0) were not especially stable in bulk oxides, being a bit more stable in MgO as compared to CaO. These defects easily trap electrons from surrounding media and collapse into more stable V^- or V^{2-} configurations. The stability of V^0 centers seems to increase for nanostructured oxides. Using photoluminescence and positron annihilation spectroscopy, the concentration of Mg vacancies was found to decrease with increasing particle size accompanied by a decrease in the saturation magnetization of the samples, with defects mostly found at the surface of the nanocrystalines [44]. The very existence of the local magnetic moment in these structures allowed one to consider MgO and CaO as strong candidates for the so-called "d^0 magnets" [43], a fascinating class of magnetic materials containing no d- or f-shell atoms.

During recent years there appeared quite a number of *ab initio* studies devoted to magnetic properties of defective MgO [34,46,47] and CaO [48]. In many reported calculations standard DFT approximations, such as the local density (LDA) and generalized gradient approximations (GGA), were used. They obtained metallic or semimetallic state for MgO and CaO with V centers, thus failing to describe the experimental observations. The magnetic state associated with cation vacancy obtained in these calculations was a spin triplet state ($S = 1$) [34,46,47].

As mentioned above, in order to reproduce the configuration with holes localized at two oxygen atoms next to the V^0 center,

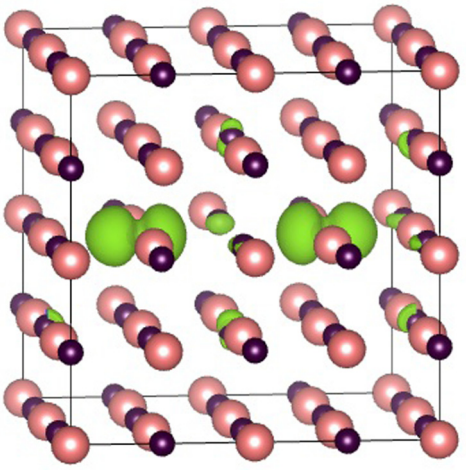

FIG. 1. (Color online) Charge distibution showing the hole localization around a cation vacancy in bulk MgO obtained in DFT + U calculations.

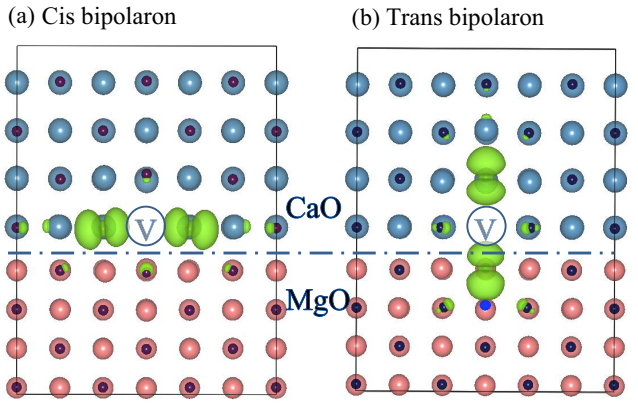

FIG. 2. (Color online) Two different bipolaron topologies at the MgO/CaO interface. (a) *cis* bipolaron is situated in the epitaxial plain. (b) *trans* bipolaron situated perpendicularly to the epitaxial plain.

one needs to use methods going beyond conventional local and semilocal approximations of DFT [34]. The key factor leading to the formation of a localized state is the local lattice distortion around the atoms where holes localize [34], thus demonstrating the paramount importance of charge-lattice interaction for the polaron formation. This distortion is reproduced by neither LDA nor GGA; both functionals result in the metallic state for MgO and CaO with V^0 centers [34,46,47]. According to Heyd-Scuseria-Ernzerhof (HSE) and SIC calculations the ferromagnetic ($S = 1$) and antiferromagnetic ($S = 0$) spin orientations for the localized holes associated with Mg vacancy differ in energy only by 1–2 meV [34]. Attempts to calculate the magnetic exchange interaction for this case using HSE and SIC resulted in the energy difference of 1 meV (HSE) and 33 meV (SiC) for defects separated by 8.34 Å [34]. Recently, Uchino and Yoko [49] reported HSE results for low-coordinated surface atoms of MgO, for which they found strong preference for ferromagnetic orientation and even suggested the formation of ferromagneticlike domains. The low-coordinated surface sites were also previously suggested as exciton traps in MgO [18].

Here, we study the formation of cation vacancy in bulk MgO and CaO and at the epitaxial (100) interfaces between these oxides. An interface breaks the local symmetry. Therefore two topological configurations of localized holes or bipolaron are possible: along and perpendicular to the interface. In the former case, both oxygen atoms of the bipolaron are situated in the layer of the same oxide on one side of the interface whereas for the latter one of the bipolaron centers is in MgO and the other one is in the CaO layer. We show these topologies in Fig. 2. In the following, bipolarons situated parallel and perpendicular to the interface plane will be called *cis* and *trans* bipolarons, respectively. Due to a considerable lattice mismatch, an ideal epitaxial interface between MgO and CaO is rather a model than reality, however, less perfect interfaces between the two oxides are grown routinely [10]. In particular, it was shown that the large lattice mismatch could be balanced out using a low-temperature buffer technique, where edge dislocations could slip along the interface [50]. Metastable nonstoichiometric MgO-CaO solutions with arbitrary lattice parameter were also grown on a MgO substrate by cold molecular beam epitaxy [51]. The chemical solution deposition was proposed as a method to create a network of CaO microislands on MgO [52]. In all cases, the interface between the two oxides naturally contains a large amount of structural defects, one type of which we investigate here.

In particular, we study how the formation energy of cation vacancy depends on the respective thickness of MgO and CaO layers and what the preferred hole localization pattern for different interfaces could be. We find that holes prefer to localize in O^1-O^1 bipolaron configurations. Although, one-center O^2-O^0 bipolaron [further for simplicity called monopolaron (MP)], where two holes localize at the p orbitals of one and the same oxygen atom are found to be metastable. Therefore their existence in defective MgO and CaO is possible. The energy barriers for bipolaron-to-monopolaron transitions are calculated and analysed for a number of chosen configurations.

The paper is structured as follows. In Sec. II, the details of calculations are presented. Section III contains our results for bulk MgO and CaO obtained with DFT + U and hybrid functionals. The bilopolarons formed at the (100) MgO/CaO interface, different hole topologies and energy barriers associated with transitions between these configurations are discussed in Sec. IV. Section V concludes our work.

II. DETAILS OF COMPUTATION

The calculations were performed in the framework of density functional theory (DFT) using the projector augmented-wave method (PAW) [53–56]. The DFT + U [57] approach using generalized gradient approximation (GGA) in the Perdew, Burke, and Ernzerhof (PBE) [58] parameterization as well as the screened hybrid functional of Heyd, Scuseria, and Ernzerhof (HSE) [59–61] were used to account for the exchange-correlation interaction. Both DFT + U and HSE were applied to study bulk oxides but only DFT + U was used in interface calculations. In the HSE approximation, the full Coulomb potential $1/r$ can be substituted by a screened one.

The Coulomb potential is divided into a short and long range parts: $1/r = S_\mu(r) + L_\mu(r) = [erfc(\mu r)]/r + [erf(\mu r)]/r$, where μ is a screening parameter. The exchange-correlation term then looks as

$$E_{xc}^{\mathrm{HSE}} = aE_x^{\mathrm{HF,SR}}(\mu) + (1-a)E_x^{\mathrm{PBE,SR}}(\mu) + E_x^{\mathrm{PBE,LR}}(\mu) + E_c^{\mathrm{PBE}}, \quad (1)$$

where μ can be varied from 0, that would correspond to PBE0 approximation [59], to infinity, that would correspond to PBE [58]. As the optimal value of this parameter differs for different materials [62], we varied this parameter in a reasonable range to find values optimal for MgO and CaO (see results below). The parameter "a" is the HF mixing constant. Although, the value of $a = 0.25$ was shown to be optimal for atoms and molecules [60–62] we show that the variation of this parameter can influence the polaron properties. The HSE calculations were carried out for bulk structures using a $2 \times 2 \times 2$ unit cell with the Γ point for the Brillouin zone integration.

As the HSE approach is rather computationally demanding DFT + U with Hubbart U applied to the p states of oxygen was also used. Although, U is usually applied to d and f states, its application to the p states of oxygen has been quite successful [13,34,63,64].

The value of U_{eff} was varied from 0 to 12 eV in the bulk calculations of the oxides. The bulk DFT + U calculations were performed for the $3 \times 3 \times 4$ unit cells using a Γ-point centered $3 \times 3 \times 2$ k-point grid. Based on the results of these tests $U = 10$ eV was chosen for the interface calculations. We notice that $U = 10$ eV was also previously applied to the p states of TiO_2 as the value providing a proper hole localization [13]. All the calculations were spin-polarized with the cutoff energy of 550 eV. The following orbitals were treated as valent states: $2p6,3s2$ (Mg), $3s2,3p6,4s2$ (Ca), and $2s2,3p4$ (O).

The (100) MgO/CaO interfaces were modelled using $3 \times 3 \times 4$ unit cells, therefore, the total number of oxide layers in the z direction was eight. Starting from pure MgO, the MgO layers were one by one substituted by the layers of CaO. As a result, we obtained seven systems with different number of MgO and CaO layers. The cell parameters and internal coordinates were fully optimized for each of these structures before creating any cation vacancy. Further, the internal coordinates were optimized for the cells containing a vacancy. The relaxation procedure was stopped when the accuracy of the total energy reached 10^{-5} eV and the Hellmann-Feynman forces were smaller than 10^{-4} eV/Å.

The cation vacancy formation energies E_{form} were calculated as

$$E_{\mathrm{form}} = E_{(\mathrm{Mg,Ca})_x O_x} - E_{(\mathrm{Mg,Ca})_{(x-1)}\mathrm{O}_x} - E_{1(\mathrm{Mg,Ca})[\mathrm{solid}]}, \quad (2)$$

and the deformation contribution to the E_{form} was estimated as the energy difference of unrelaxed (E_{unrel}) and fully relaxed (E_{rel}) cells with different polaron topologies.

III. RESULTS AND DISCUSSION

A. Hole bipolarons in bulk MgO and CaO

First, we discuss our results for a cation vacancy in bulk MgO and CaO obtained with DFT + U and HSE functionals. To calibrate DFT + U we varied U_{eff} from 0 to 12 eV.

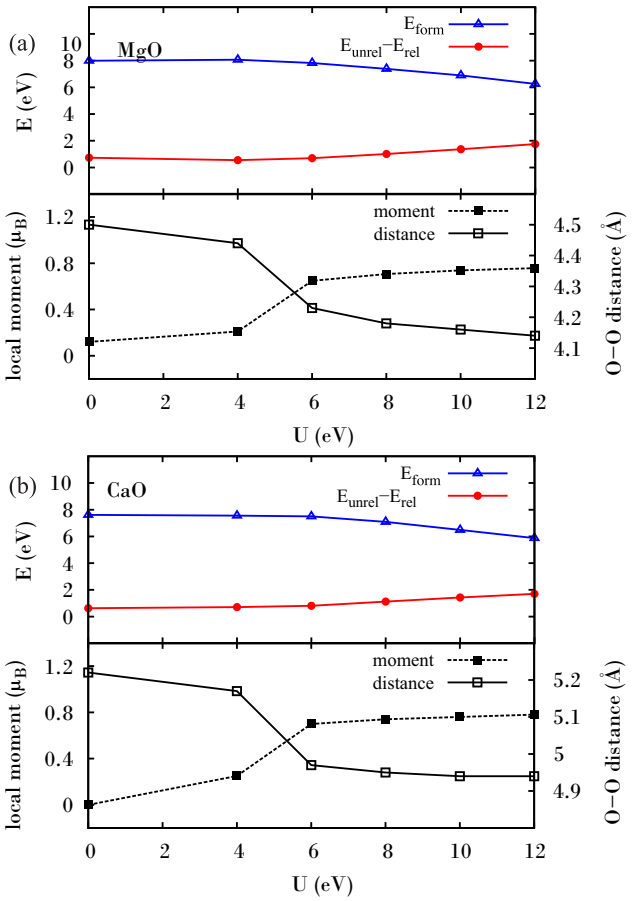

FIG. 3. (Color online) Characteristics of bipolaron as a function of U_{eff}. Top panels show vacancy formation energies E_{form} and deformation contribution ($E_{\mathrm{unrel}} - E_{\mathrm{rel}}$) to E_{form}. The bottom panels show the localised magnetic moment on each oxygen with an unoccupied state and the characteristic O-O distance.

The equilibrium lattice parameter decreases with increasing U_{eff} from 4.26 Å ($U_{\mathrm{eff}} = 0$) to 4.20 Å ($U_{\mathrm{eff}} = 12$ eV) for MgO and from 4.84 Å ($U_{\mathrm{eff}} = 0$) to 4.80 Å ($U_{\mathrm{eff}} = 12$ eV) for CaO. In Fig. 3, we show vacancy formation energies, magnetic moments, and the distances between the two oxygens where holes are localized, as a function of U_{eff}. The vacancy formation energy in MgO decreases from 7.99 eV for $U_{\mathrm{eff}} = 0$ to 6.26 eV for $U_{\mathrm{eff}} = 12$ eV [Fig. 3(a)]. In CaO, the formation energy ranges from 7.61 ($U_{\mathrm{eff}} = 0$ eV) to 5.87 eV ($U_{\mathrm{eff}} = 12$ eV) [Fig. 3(b)]. Furthermore, in between $U_{\mathrm{eff}} = 4$ and 6 eV the slope of the energy curve slightly changes [Figs. 3(a) and 3(b)]. The changes in the behaviour of the magnetic moment and O-O distance, occurring in this rage of U_{eff}, are even more noticeable [Figs. 3(a) and 3(b)]. The increase of the magnetic moment and drop in the O-O separation indicates the minimum value of U_{eff}, which can provide a relatively full hole localization at two opposite oxygen atoms. In the density of states (DOS) this is seen as a split-off feature from the valence band, providing an unoccupied mid-gap state in the spin-down channel (see Fig. 4). Droghetty *et al.* [34], estimated that $U_{\mathrm{eff}} = 5$–7 eV is a proper range providing a correct hole topology in MgO, and this is consistent with our results. Further increase of U_{eff} up to 12 eV does not change this picture

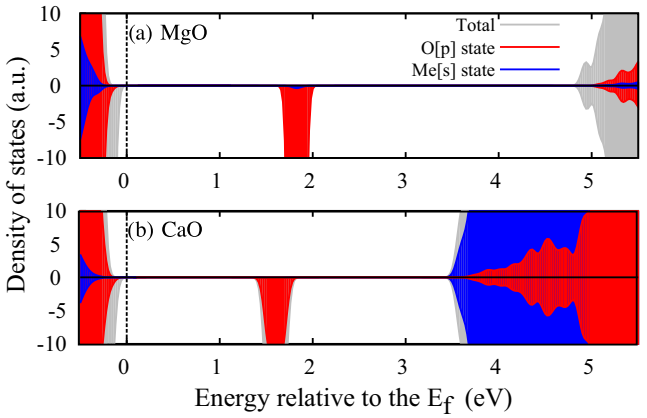

FIG. 4. (Color online) Density of states for MgO and CaO supercells with a V^0 center (DFT + U calculation, $U_{\text{eff}} = 12$). An unoccupied O_p state in the mid-gap indicates hole localization in both oxides.

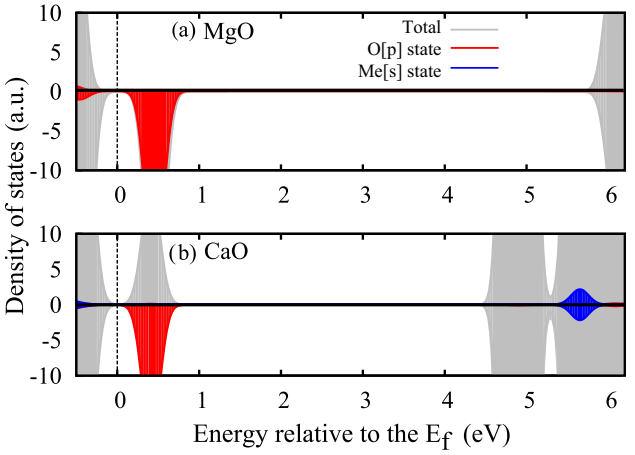

FIG. 5. (Color online) DOS curves obtained in HSE calculations ($a = 0.25$, $\mu = 0.2$). For CaO the singlet configuration is the ground state as the unoccupied mid-gap states are present for both spin-down (partial DOS, red) and spin-up (total DOS, grey) channels.

qualitatively, just slightly increasing the degree of localization and pushing the empty p states further up in the band gap.

Based on this analysis we choose $U_{\text{eff}} = 10$ eV for our interface calculations. In this case, the equilibrium lattice parameters are 4.21 Å (MgO) and 4.81 Å (CaO), close to the experimental values of 4.207 Å (MgO) and 4.803 Å (CaO) [65]. For MgO, the O-O distance of the bipolaron is about 4.16 Å, that is smaller than the O-O separation of the matrix oxide (4.21 Å). In the case of CaO, the O-O separation in the bipolaron is 4.94 Å, that is larger than 4.81 Å, the O-O distance in the perfect oxide. The DOS curves calculated for MgO and CaO with $U_{\text{eff}} = 10$ eV are shown in Fig. 4. The band gap for MgO obtained with $U_{\text{eff}} = 10$ is 4.8 eV as compared to the experimental value of 7.67 eV [66], showing the common underestimation of the band gap of DFT based calculations. The separation between the unoccupied hole states and the top of the valence band is 1.7 eV. For CaO, the calculated gap is 3.4 eV as compared to the experimental value of 6.93 eV [66] with the empty impurity level situated 1.4 eV above the top of the valence band Fig. 4. The presented DOS curves demonstrate the triplet solution, which is lower in energy by 1 meV compared to the singlet one.

For comparison, the cation vacancies in bulk MgO and CaO were also calculated using a hybrid functional (HSE). Similar to DFT + U, the HSE approach has parameters, which can be system specific, in particular, the Hartree-Fock (HF) mixing parameter "a" and the screening radius μ [see Eq. (3)]. First, we assume $a = 0.25$ and $\mu = 0.2$. Calculated DOS curves show that the bipolaronic character of hole localization, associated with cation vacancy, is again reproduced for both oxides. In MgO, the obtained equilibrium magnetic configuration is the triplet, which is by 11 meV lower in energy than the singlet state. The hole states are 0.42 eV above the top of the valence band, see Fig. 5. However, in contrast to MgO, the singlet state is found to be most stable (by 20 meV) in CaO, which is also in agreement with experimental observations [36,45]. The states corresponding to the singlet solution are 0.38 eV above the top of the valence band, both in spin-up and spin-down channels (Fig. 5). Hence it seems that both DFT + U and HSE methods produce localized hole solutions with similar degree of localization in agreement with previous results [34]. We notice that the magnetic moments obtained in the HSE calculations with $a = 0.25$ are smaller than those from the DFT + U calculations. We find that they are directly affected by the value of the HF admixing parameter "a". The calculations show that the on-site magnetic moment steadily increases with increasing HF contribution reaching 0.77 μ_B for both oxides. The increase of the "a" parameter shifts an empty hole p states up in the band gap, which in its turn increases the width. For example, the values for the band gap obtained in calculations with $a = 0.25$ change from 5.82 eV (MgO) and 4.52 eV (CaO) to 7.52 eV (MgO) and 6.12 eV (CaO) for $a = 0.5$.

Next, we study the character of hole localisation with variable screening radius μ. There, we assume the HF mixing parameter $a = 0.25$ and vary μ from zero, that corresponds to the PBE0 functional, to $\mu = 2$, the value considered as the PBE limit ($\mu = \infty$). In this range, the equilibrium lattice parameter varies from 4.25 Å ($\mu = 2$) to 4.20 Å ($\mu = 0.2 - 0$) for MgO and from 4.85 Å ($\mu = 2$) to 4.82 Å ($\mu = 0.2$–0) for CaO. Figure 6(a) presents the formation energies, magnetic moments and O-O distances calculated for MgO with different values of μ. Similar information is shown for CaO in Fig. 6(b). The formation energy shows a slight increase when the screening radius reaches 0.2 from above and further stays virtually the same as it approaches zero. The magnetic moment and O-O distance show more pronounced changes at $\mu = 0.2$–0.3 indicating the transition between delocalized and localized solutions. Calculations with μ in the range from 0.2 to 0 give stable geometry for the bipolaron with characteristic distances between the bipolaron centers of 4.21 and 4.93 Å and local magnetic moments of 0.56 μ_B and 0.69 μ_B for MgO and CaO, respectively (see Fig. 6). Comparing our HSE and DFT + U results, Figs. 3(a), 3(b), and 6(a), 6(b), we notice that in both cases, we observe an increase of magnetic moment and decrease of the O-O distance in the bipolaron pair as we go away from pure PBE

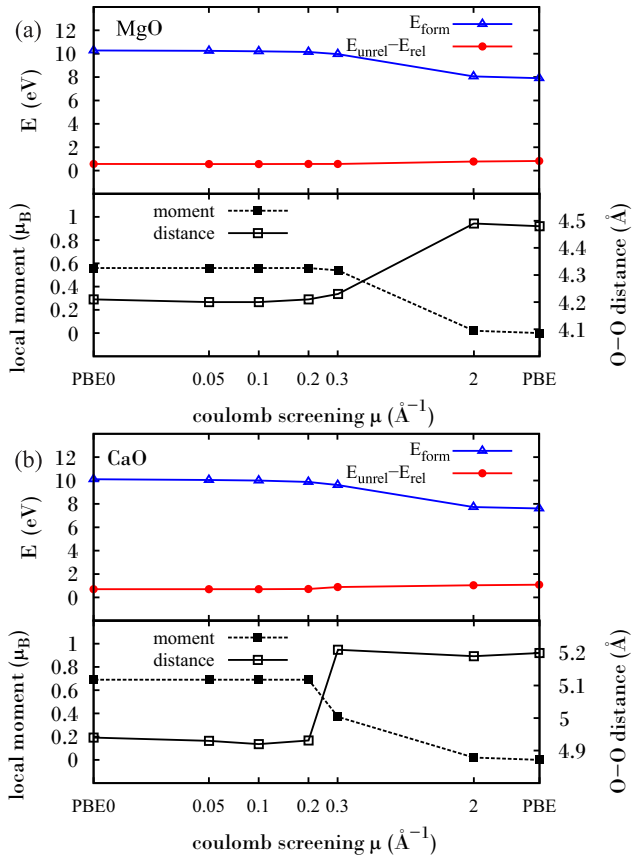

FIG. 6. (Color online) Bipolaron properties obtained within hybrid functionals. Data are presented as a function of Coulomb screening μ.

description. However, different from PBE + U, where the vacancy formation energy becomes smaller with growing U, for HSE, we observe a slight increase of E_{form} as μ decreases.

The HSE functional is often viewed as an approach less dependent on free parameters compared to DFT + U. However, the latter is significantly less computationally demanding and this makes it preferable when large systems need to be considered. It is known that semilocal DFT approximations do not reproduce the correct linear behaviour of energy for fractional occupations [67,68] that might result in slightly wrong charge redistributions. However, as we do not study optical excitations in this work the error introduced by this shortcoming of DFT is expected to have a minor effect on the phenomena considered here.

B. Hole bipolarons at the (100) MgO/CaO interfaces

To understand the effects of anisotropy on the polaron formation, we have systematically studied cation vacancies and associated hole localization for seven different interfaces, where the relative Mg/Ca concentration is varied by changing the number of MgO and CaO layers (see Fig. 7 for illustration). Figure 7 also presents the strain for the defect free interfaces obtained after a full relaxation of the unit cell. In all the studied interface structures, MgO appears to be stretched in-plane whereas CaO is always compressed in-plane [Fig. 7(a)]. In the direction perpendicular to the interface, CaO is compressed

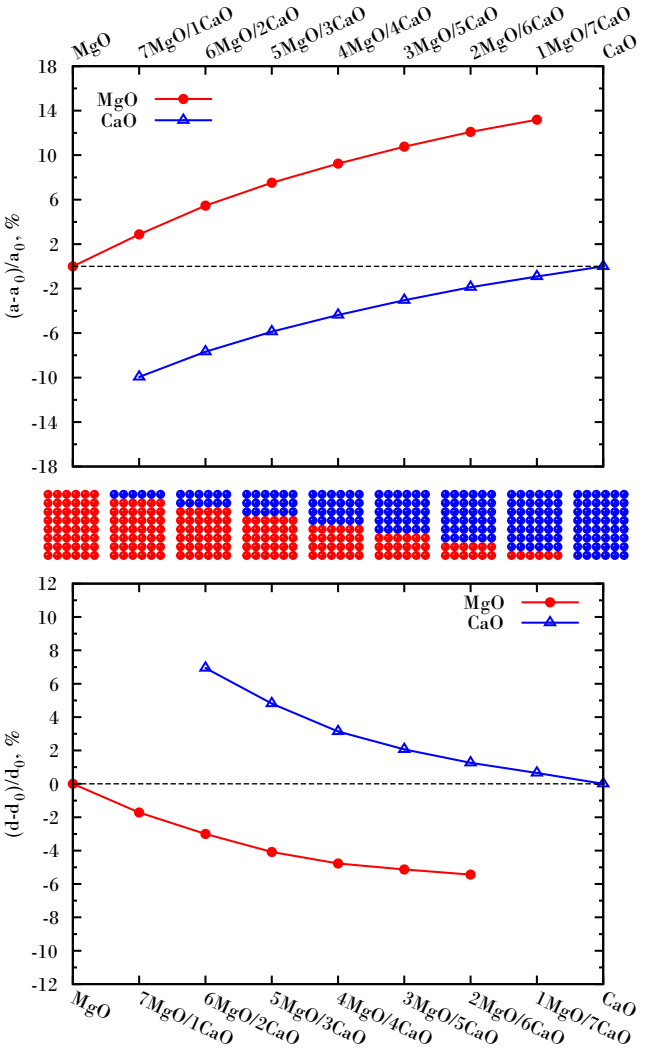

FIG. 7. (Color online) Calculated lateral (a) and transverse (b) strains of MgO and CaO in the cells of various compositions.

whereas MgO is stretched [Fig. 7(b)]. Hence, the formation of an interface between MgO and CaO results in opposite sign of the lateral and transverse strains of both materials.

At the interface, one can have two types of cation vacancies: in the interface MgO layer or interface CaO layer. Additionally, the interface anisotropy provides two bipolaronic topologies for each vacancy type: a *cis* configuration when the bipolaron lies in the interface plane [Fig. 2(a)] and a *trans* configuration when the bipolaron is perpendicular to the interface [Fig. 2(b)]. Therefore, for each interface composition, we have four bipolaronic configurations to consider. In Fig. 8, the vacancy formation energies with *cis* and *trans* bipolarons are presented. There are several things to notice. First of all, the energy of the Mg vacancy formation decreases substantially as the MgO film becomes thinner that is from 6.88 eV for pure MgO to 4.31 eV for the case of the MgO monolayer in the *cis* geometry [Fig. 8(a)]. In addition, the formation energy of the *trans* polaron is higher than that of *cis* for all thicknesses of MgO.

At the same time, the formation energy of Ca vacancy shows no pronounced change with thickness, exhibiting only

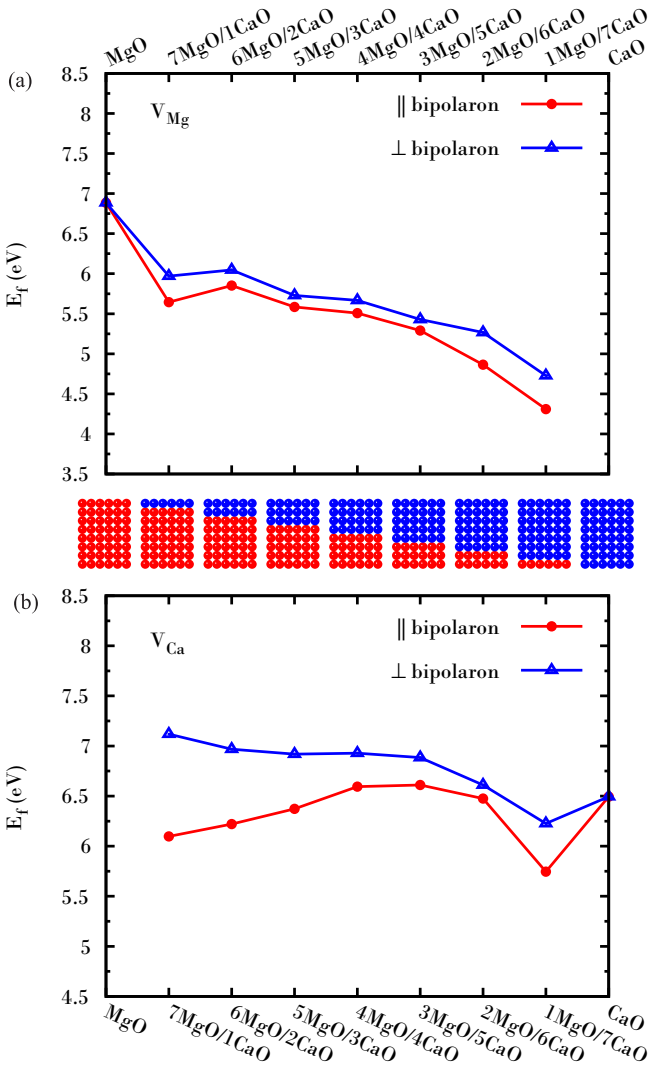

FIG. 8. (Color online) Formation energy of cation vacancies situated at the MgO/CaO interface either in the MgO (a) or CaO (b) layer calculated for different bipolaron topologies [*cis* (∥) and *trans* (⊥)].

slight variation within ±0.5 eV when the thickness changes [Fig. 8(b)]. The energy required to form a Mg vacancy is smaller than that for a Ca vacancy in most of the cases. Furthermore, the formation energies appear to be rather sensitive to the bipolaronic configuration with the energy minimum corresponding to the *cis* geometry in the whole composition range (Fig. 8). To make sure that the observed trends do not crucially depend on the lateral size of the unit cell we performed Γ point calculations for the 4 × 4 × 4 4ML-MgO/4ML-CaO supercell. For a Mg vacancy, the energy of the *cis* configuration is 0.20 eV lower than that of *trans* bipolaron that is close to the value obtained for the 3 × 3 × 4 supercell (0.16 eV). For a Ca vacancy, the energy differences between *cis* and *trans* are 0.36 and 0.34 eV for 4 × 4 × 4 and 3 × 3 × 4 cell, respectively.

Therefore the holes prefer to localize at the oxygen pair situated parallel to the interface in the same material where the cation vacancy is formed (Fig. 8). The difference between the *cis* and *trans* configurations is at most 0.5 eV for MgO but it reaches 1 eV for thinner CaO layers.

The formation of a cation vacancy and the accompanied hole localization lead to substantial local distortions of the oxide matrix. To estimate how far these distortions spread in the lattice, we calculated the distances from each atom to the bipolaronic center in distorted R and undistorted R_0 crystals. If we include all the atoms for which $R_0 - R$ is larger than 0.005 Å into the distorted area we find that in the case of Mg vacancy the distortion radius is about 5–7 Å for both *cis* and *trans* configurations. The distorted area is somewhat larger in the case of Ca vacancy, for which the radius can reach 10 Å, if calculated with the same procedure.

At interfaces a polaron formation is influenced by both strain and electronic anisotropy. To estimate the importance of these factors we carried out an additional series of calculations. In the bipolaronic configurations obtained for the Mg vacancy we replaced all Ca atoms in the CaO layers by Mg atoms, then, keeping the geometry fixed we performed one self-consistent cycle to obtain the total energy. The same procedure was repeated for the Ca vacancy replacing all Mg atoms with Ca. In this way we removed the interface and corresponding electronic anisotropy while preserving the lattice strain. The resulting total energies are shown in Fig. 9. In the case of a vacancy in MgO the anisotropy of *cis* and *trans* configurations almost disappears when the interface is removed [Fig. 9(a)]. We still observe a decrease of the vacancy formation energy with growing in-plane strain to 4.5 eV that is comparable to the trend obtained in the system with the MgO/CaO interface [compare Fig. 8(a) and Fig. 9(a)].

In the case of CaO we see a different behaviour, the anisotropy does not disappear when MgO is removed, moreover, the *trans* configuration becomes energetically more favourable than *cis*, so the trend is reversed compared to the system with an interface [compare Figs. 8(b) and 9(b)]. It seems that deformations, which are different for the *cis* or the *trans* configurations, could contribute to the observed behaviour. For the larger 4 × 4 × 4 cell, this effect appears to be even more pronounced. Our calculations for the 4 × 4 × 4 4ML-MgO/4ML-CaO supercell using the Γ point show that for this cell the *trans* configuration is preferred over *cis* by 1.53 eV, which should be compared to 1.24 eV we obtained for the 3 × 3 × 4 CaO slab. In the case of the interface free 4 × 4 × 4 MgO slabs, the difference between *cis* and *trans* again is small (0.067 eV). Interestingly, when Mg atoms are removed the general trend for the formation energy of Ca vacancy is to decrease as the strain level increases (see Fig. 9). This is similar to the trend found for Mg vacancies [Figs. 8(a) and 9(a)] but very different from the behavior observed for Ca vacancies at MgO/CaO interfaces [compare Figs. 8(b) and 9(b)].

The equilibrium magnetic configuration obtained for all the considered bipolaronic configurations is the triplet state ($S = 1$). We checked the stability of the singlet state ($S = 0$) using the 4ML-MgO/4ML-CaO slabs for Mg and Ca vacancy with bound *cis*/*trans* bipolarons. Our calculations show that the singlet state is only 1–2 meV higher in energy than the triplet state. Thus the two magnetic states are virtually degenerate, the finding that agrees well with our bulk calculations as well as previously reported theoretical and experimental results [41,68]. Generally, it is an interesting result as simple models

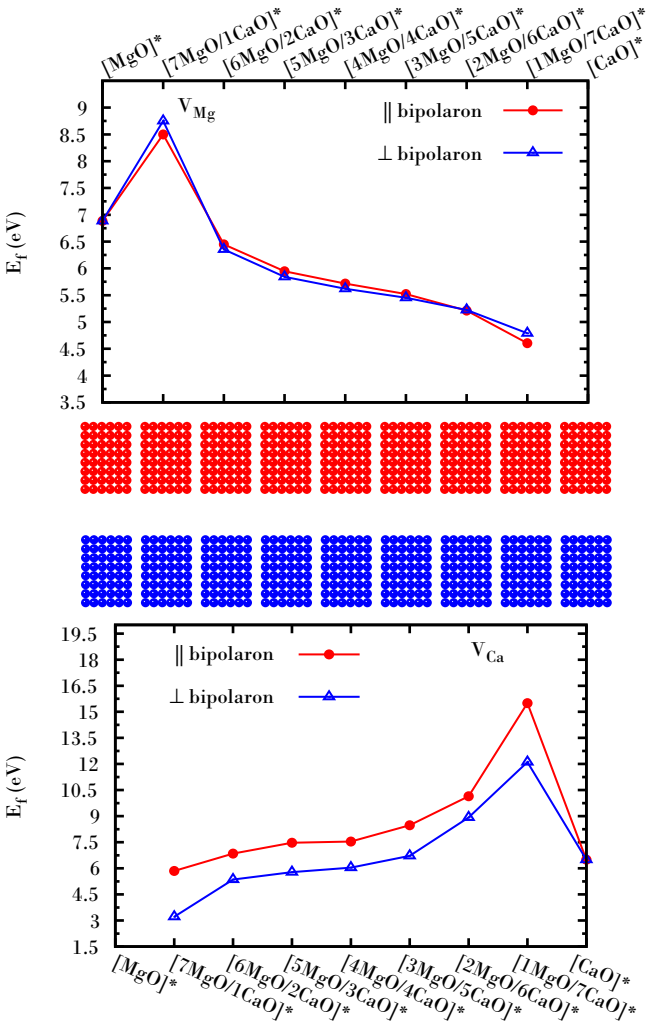

FIG. 9. (Color online) Same data as shown in Fig. 8 but for interface free calculations. Notice the opposite trends as compared to those shown in Fig. 8. Labels marked with asterisk indicate the character of the cell deformation induced upon the interface free slabs.

of a two electron system placed in a potential always give the singlet configuration as the ground state [69]. Some exotic models were put forward in an attempt to reconcile simple model predictions and experimental observations. In particular, it was suggested that an admixture of O^2-O^0 state into the dominant O^1-O^1 is able to stabilize the triplet solution [41].

IV. TRANSITIONS BETWEEN DIFFERENT POLARONIC CONFIGURATIONS

Here, we study the possibility for one-center O^2-O^0 bipolaron [here called monopolaron (MP)] to exist at the MgO/CaO interfaces as well as possible hole transitions between different polaronic configurations.

The monopolaron is not the ground state and could have a rather high energy. In order to stabilize it, we take advantage of the fact that the deformation pattern around the localized charge is of a paramount importance for the

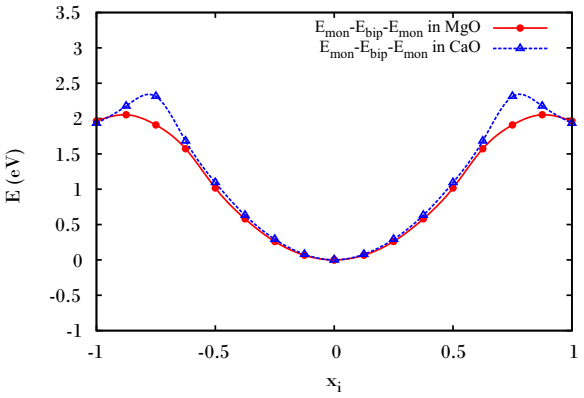

FIG. 10. (Color online) Monopolaron-bipolaron-monopolaron transition estimated in the linear approximation [see Eqs. (3) and (4)] in pure oxides. Initial and final configurations are equivalent due to symmetry ($x = -1$ and 1). We choose to shift all energies in such a way that $E_{\rm bip}^{\rm MgO} = E_{\rm bip}^{\rm CaO} = 0$.

polaron stabilization. To prepare the initial guess for the local atomic configuration around the monopolaron, we introduced a lattice distortion into the unit cell around one of the oxygens neighbouring the cation vacancy, and we obtained a metastable local energy minimum. The unit cell was then fully relaxed. After the relaxation we obtained a metastable O^2-O^0 polaronic configuration. First, we did this excise for bulk MgO and CaO and obtained monopolaronic lattice configurations for both oxides, whose energy was about 2 eV higher than that of the O^1-O^1 ground state, as shown in Fig. 10.

Further, we calculated the energies for the bipolaron-to-monopolaron transition modelled in a linear approximation, which roughly estimates the energy barriers for hole migration using the set of cell configurations obtained with the linear interpolation procedure [24,32]. Each atomic coordinate is specified with a parameter q, and a given set of atomic coordinates is then specified by $\sum q^p$. We introduce a superscript for the monopolaron and bipolaron configurations, and specify these two polarons with the configurations $\sum q^m$ and $\sum q^b$, respectively. A linear interpolation of these configurations can then be written as

$$\sum q^p = -x \sum q^{m1} + (1+x) \sum q^b,$$

$$-1 < x < 0. \qquad (3)$$

This expression describes the transition between the monopolaron configuration where two holes are located on the oxygen atom on one side of the vacancy (denoted as m1 configuration). The configuration where the two holes are on the oxygen atom on the other side of the vacancy, is denoted as m2, and the transition from the bipolaron to the monopolaron state m2, is calculated as

$$\sum q^p = (1-x) \sum q^b + x \sum q^{m2},$$

$$0 < x < 1. \qquad (4)$$

The resulting energies for bulk MgO and CaO are shown in Fig. 10. The bipolaron configuration is at 0 and monopolarons at (-1) and (1) according to the notation chosen here. The

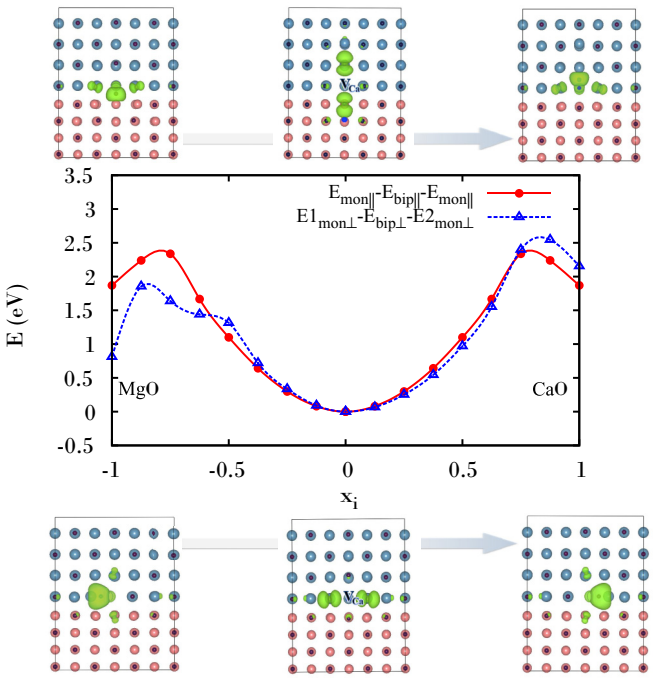

FIG. 11. (Color online) Total energies of the monopolaron-bipolaron-monopolaron path, defined in Eqs. (3) and (4), as $x = -1 \rightarrow x = 0 \rightarrow x = 1$, calculated for the case of the interface Ca vacancy. Both *cis* and *trans* polarons are considered. In the top and bottom figures, charge densities corresponding to different polaronic configurations are shown.

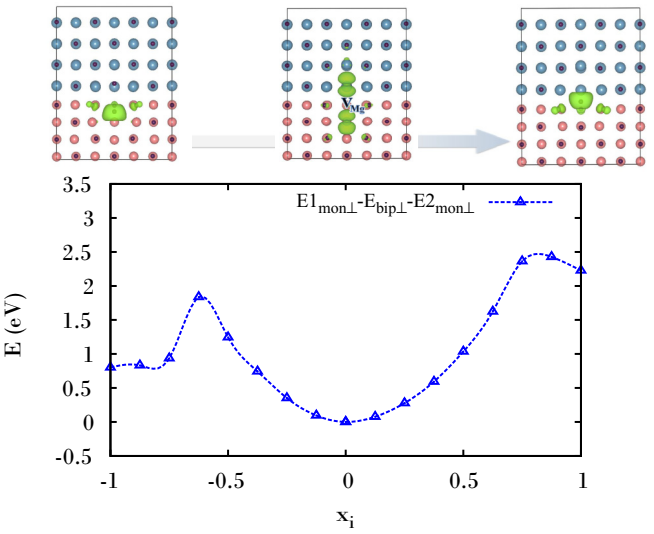

FIG. 12. (Color online) Total energies of the monopolaron-bipolaron-monopolaron path, defined in Eqs. (3) and (4), calculated for the interface Mg vacancy. We only show the transition for the *trans* bipolaron as the *cis* configuration could not be stabilised.

curves are symmetric as in bulk O^2-O^0 and O^0-O^2 configurations are equivalent. The monopolaronic configuration is metastable in both oxides showing a noticeable energy barrier(0.5 eV) in the case of CaO. The bipolaronic solution is separated from the monopolaronic one by a barrier of approximately 2.5 eV.

To study polaronic transitions at the MgO/CaO interface we chose the 4ML-MgO/4ML-CaO system. For the Mg and Ca vacancies, we considered three transitions: *cis* bipolaron to monopolaron, which is centerd at an oxygen of the initial O^1-O^1 pair; *trans* bipolaron to monopolaron centered at one oxygen of the initial O^1-O^1 pair situated either in CaO or in MgO layer. We obtained the energies for the transitions involving both *cis* and *trans* configurations in the case of Ca vacancy, shown in Fig. 11, but only for the *trans* geometries in the case of Mg vacancy, shown in Fig. 12. The curve is symmetric for the transition involving *cis* configurations but asymmetric in the *trans* cases as monopolarons form in different materials. The monopolaronic solution is metastable for both Mg and Ca vacancies and its stability is enhanced at the interface as indicated by a deepening of the corresponding energy minima, especially noticeable for MgO (compare Figs. 10 and 11). The monopolarons formed in the CaO layer have lower energy compared to those formed in MgO and generally are more stable. The barriers for the *cis* bipolaron-to-monopolaron transition is just slightly lower than those in bulk CaO (Fig. 11). The barriers for transitions involving the *trans* bipolaron are lower for the transition to the monopolaron placed in CaO than those in MgO: 1.5 and 1.9 eV for Ca and Mg vacancies, respectively. The barriers for the transition to the monopolaron placed in MgO are somewhat larger: 1.9 and 2.5 eV for Ca and Mg vacancies, respectively.

We notice that the linear approximation is expected to substantially overestimate the transition barriers and can be used primarily as an indication. The calculations do not provide the life time of the states, neither take into account probable tunnelling between different states. Nonetheless, our results indicate a possibility for monopolaronic topologies to exist as metastable states therefore one cannot rule out their presence in MgO/CaO samples.

V. CONCLUSION

To summarize, we have modelled different hole bipolaronic configurations around a cation vacancy at the (100) MgO/CaO interface. The vacancy formation is substantially facilitated by the presence of the interface. We applied two theoretical methods, DFT + U and HSE hybrid functional, and this allowed us to obtain a correct hole localization pattern provided the local lattice distortion around the defect is accurately described. The O^1-O^1 bipolaronic configuration is found to be the ground state in all the studied cases. At the interface the *cis* configurations are always preferred. The triplet and singlet magnetic configurations are degenerate within the accuracy of 1–2 meV. The O^2-O^0 bipolaronic solution is metastable exhibiting deeper local minima at the interface compared to those in bulk oxides. This result indicates that different bipolaronic configurations could coexist at the MgO/CaO interfaces.

ACKNOWLEDGMENTS

We acknowledge the financial support by the Swedish Energy Agency (Energimyndigheten, STEM) eSSENCE, STANDUPP and the Swedish Research Council

(Vetenskapsrådet). Supercomputer time was granted by the Swedish National Infrastructure for Computing (SNIC). N.B. is grateful to A. Belonoshko and S. Arapan for valuable discussions and to P. Larsson for technical support. O.E. Acknowledges in addition the KAW foundation and the ERC (ASD project 247062).

[1] L. D. Landau, Phys. Zeit. Sowjetunion (J. Physics (USSR)) **3**, 664 (1933).
[2] S. I. Pekar, Zh. Eksp. Teor. Fiz. **16**, 335 (1946).
[3] H. Fröhlich, Adv. Phys. **3**, 325 (1954).
[4] T. Holstein, Ann. Phys. (N. Y.) **8**, 325 (1959).
[5] J. T. Devreese, *in Encyclopedia of Applied Physics*, edited by G. L. Tigg (Wiley-VCH, Weinheim, 1996).
[6] A. S. Alexandrov and N. F. Mott, *Polarons and Bipolarons* (World Scientific, Singapore, 1996).
[7] A. S. Alexandrov and J. Ranninger, Phys. Rev. B. **23**, 1796 (1981).
[8] D. Emin and M. S. Hillery, Phys. Rev. B. **39**, 6575 (1989).
[9] A. S. Alexandrov and N. F. Mott, *High Temperature Superconductors and Other Superfluids* (Taylor and Francis, London, 1994).
[10] T. Maxisch, F. Zhou, and G. Ceder, Phys. Rev. B. **73**, 104301 (2006).
[11] N. V. Skorodumova, S. I. Simak, B. I. Lundqvist, I. A. Abrikosov, and B. Johansson, Phys. Rev. Lett. **89**, 166601 (2002).
[12] O. Hellman, N. V. Skorodumova, and S. I. Simak, Phys. Rev. Lett. **108**, 135504 (2012).
[13] N. A. Deskins, R. Rousseau, and M. Dupuis, J. Phys. Chem. C **113**, 14583 (2009).
[14] P. E. Spencer, J. H. Samson, P. E. Kornilovitch, and A. S. Alexandrov, Phys. Rev. B. **71**, 184310 (2005).
[15] A. S. Alexandrov and N. F. Kornilovich, Phys. Rev. Lett. **82**, 807 (1999).
[16] A. M. Stoneman, J. Phys. C: Solid State Phys. **3**, L131 (1970).
[17] H. Fehske, J. Loos, and G. Wellein, Phys. Rev. B. **61**, 8016 (2000).
[18] E. Cappelluti, S. Ciuchi, and S. Fratini, Phys. Rev. B. **79**, 012502 (2009).
[19] M. Nolan and G. W. Watson, Surface Science C **586**, 25 (2005).
[20] A. Walsh, C. R. A. Catlow, M. Miskufova, and A. A. Sokol, J. Phys.: Condens. Matter **23**, 334217 (2011).
[21] J. L. Lyons, A. Janatti, C. G. Van de Walle, Journal of Appl. Phys. **115**, 012014 (2014).
[22] M. Nolan and G. W. Watson, J. Chem. Phys. **125**, 144701 (2006).
[23] P. R. L. Keating, D. O. Scanlon, and G. W. Watson, J. Phys.: Condens. Matter **21**, 405502 (2009).
[24] N. A. Deskins and M. Dupuis, Phys. Rev. B. **75**, 195212 (2007).
[25] N. A. Deskins and M. Dupuis, J. Phys. Chem. C **113**, 346 (2009).
[26] B. J. Morgan and G. W. Watson, Phys. Rev. B. **80**, 233102 (2009).
[27] A. Stashans and Y. Bravo, Mod. Phys. Lett. B **27**, 1350113 (2013).
[28] A. Janatti, C. Franchini, J. B. Varley, G. Kresse, C. G. Van de Walle, Phys. Status Solidi-Rapid Res. Lett. **7**, 199 (2013).
[29] M. Stoneham, J. Phys.: Cond. Matter **22**, 074211 (2010).
[30] K. P. McKenna *et al.*, Phys. Rev. Lett. **108**, 116403 (2012).
[31] O. F. Schirmer, M. Imlau, C. Merschjann, and B. Schoke, J. Phys.: Condens. Matter **21**, 123201 (2009).
[32] S. P. Ong, Y. Mo, and G. Ceder, Phys. Rev. B. **85**, 081105 (2012).
[33] J. M. Garcia-Lastra *et al.*, J. Phys. Chem. C **117**, 5568 (2013).
[34] A. Droghetti, C. D. Pemmaraju, and S. Sanvito, Phys. Rev. B. **81**, 092403 (2010).
[35] Y. Chen and M. M. Abraham, J. Phys. Chem. Solids **51**, 747 (1990).
[36] J. E. Wertz *et al.*, Discuss. Faraday Soc. **28**, 136 (1959).
[37] B. H. Rose and L. E. Halliburton, J. Phys. C **7**, 3981 (1974).
[38] L. A. Kappers, F. Dravnieks, and J. E. Wertz, J. Phys. C **7**, 1387 (1974).
[39] M. M. Abraham and Y. Chem, Solid State Commun. **16**, 1209 (1975).
[40] A. J. Tech and M. J. Duck, J. Phys. C **8**, 257 (1975).
[41] R. H. Bartram and A. M. Stoneham, J. Phys. C **9**, 73 (1976).
[42] P. Baranek, G. Pinarello, C. Pisani, and R. Dovesi, Phys. Chem. Chem. Phys. **2**, 3893 (2000).
[43] I. S. Elfimov, S. Yunoki, and G. A. Sawatzky, Phys. Rev. Lett. **89**, 216403 (2002).
[44] N. Kumar, D. Sanyal, and A. Sundaresan, Chem. Phys. Lett. **477**, 360 (2009).
[45] B. Henderson and A. C. Tomilinson, J. Phys. Chem. Solids **30**, 1801 (1969).
[46] F. Wang, Z. Pang, L. Lin, S. Fang, Y. Dai, and S. Han, Phys. Rev. B. **80**, 144424 (2009).
[47] F. Gao *et al.*, Solid State Commun. **149**, 855 (2009).
[48] J. Osorio-Guilln, S. Lany, S. V. Barabash, and A. Zunger, Phys. Rev. Lett. **96**, 107203 (2006).
[49] T. Uchino and T. Yoko, Phys. Rev. B. **87**, 144414 (2013).
[50] H. D. Li *et al.*, J. Appl. Phys. **102**, 046103 (2007).
[51] E. S. Hellman and E. H. Hartford, Appl. Phys. Lett. **64**, 1341 (1994).
[52] P. A. Langjahr *et al.*, J. Cryst. Growth **256**, 162 (2003).
[53] G. Kresse and J. Hafner, Phys. Rev. B. **47**, 558 (1993); **49**, 14251 (1994).
[54] G. Kresse and J. Furthmller, Comput. Mat. Sci. **6**, 15 (1996); Phys. Rev. B. **54**, 11169 (1996).
[55] P. E. Blochl, Phys. Rev. B. **50**, 17953 (1994).
[56] G. Kresse and D. Joubert, Phys. Rev. B. **59**, 1758 (1999).
[57] S. L. Dudarev, G. A. Botton, S. Y. Savrasov, C. J. Humphreys, and A. P. Sutton, Phys. Rev. B. **57**, 1505 (1998).
[58] J. P. Perdew, K. Burke, and M. Ernzerhof, Phys. Rev. Lett. **77**, 3865 (1996).
[59] J. Paier, R. Hirschl, M. Marsman, and G. Kresse, J. Chem. Phys. **122**, 234102 (2005).
[60] J. Heyd, G. E. Scuseria, and M. Ernzerhof, J. Chem. Phys. **118**, 8207 (2003); **124**, 219906 (2006).
[61] J. Heyd and G. E. Scuseria, J. Chem. Phys. **120**, 7274 (2004); **121**, 1187 (2004).

[62] O. A. Vydrov *et al*., J. Chem. Phys. **125**, 074106 (2006).
[63] J. J. Plata, A. M. Mrquez, and J. F. Sanz, J. Chem. Phys. **136**, 041101 (2012).
[64] G. Rahman, N. U. Din, V. M. Garcia-Suarez, and E. Kan, Phys. Rev. B. **187**, 205205 (2013).
[65] D. K. Smith and H. R. Leider, J. Appl. Cryst. **1**, 246 (1968).
[66] R. C. Whited, C. J. Flaten, and W. C. Walker, Solid State Commun. **13**, 1903 (1973).
[67] J. P. Perdew, A. Ruzsinszky, G. I. Csonka, O. A. Vydrov, G. E. Scuseria, V. N. Staroverov, and J. Tao, Phys. Rev. A. **76**, 040501(R) (2007).
[68] S. Lany and A. Zunger, Phys. Rev. B. **80**, 085202 (2009).
[69] C. Herring, Rev. Mod. Phys. **34**, 631 (1962).